

# Theoretical aspects and numerical modelling of the GPR method to analyse its possibilities for the detection of leakages in urban water supply networks

Tomisław Gołębiowski

*Cracow University of Technology, Faculty of Environmental Engineering and Energy,  
Department of Geoengineering and Water Management, Krakow, Poland,  
e-mail: tomislaw.golebiowski@pk.edu.pl, ORCID ID: 0000-0002-4005-2265*

© 2023 Author(s). This is an open access publication, which can be used, distributed and re-produced in any medium according to the Creative Commons CC-BY 4.0 License requiring that the original work has been properly cited.

Received: 5 March 2023; accepted: 5 September 2023; first published online: 27 October 2023

**Abstract:** Geophysical methods, especially selected electrical and electromagnetic ones, have been used for many years for the non-invasive detection of leakages from water supply networks. In this paper, the author focuses on theoretical aspects and numerical simulations to analyse the possibilities and limitations of the application of the selected electromagnetic method, i.e., the ground-penetrating radar (GPR) method for the aforementioned purpose. Various measurement techniques are used in the GPR method but in the paper the author refers to the most commonly used technique known as short-offset reflection profiling (SORP). As demonstrated in the paper, the detection of water leakages into a homogeneous and isotropic geological medium using the GPR method is a simple matter. However, the detection of leakages occurring in heterogeneous ground subjected to strong anthropopression and with the presence of electromagnetic interference becomes a difficult task, and interpretation may be difficult or even impossible. An important issue analysed in the paper was the phenomenon of the scattering of electromagnetic waves on underground anthropogenic objects, which very often occurs in urbanised areas. The results of the numerical modelling carried out for various scenarios of water leakages into typical ground allowed the possibilities and limitations of using the GPR method for the detection of leakages from water supply networks to be determined.

**Keywords:** GPR, leakage, water supply network, urbanised areas

## INTRODUCTION

Water supply networks in Poland are located between depths of ca. 1–2 m below the freezing zone (Fig. 1A) in different ground types which are usually a mixture of sand, silt, and clay (Fig. 1B). In many other countries, both the depth location of water pipes and types of grounds will be similar to those analysed in the paper; therefore, the conclusion drawn in the paper may be treated as universal.

Damage of pipe and the subsequent underground leakage of water is the most often monitored using pressure and flow sensors installed in the network nodes. Additionally, different detectors may also be used for this purpose. Geodetic observations of the movement of the earth surface as well as the monitoring of subsidence (caused by suffosion) are also useful tools for location of leakage region. For leakage detection and monitoring its impact on the ground, geophysical methods are usually applied; among the wide range of

geophysical methods available for the detection of water leakage, mainly selected electrical (i.e. ERT – electrical resistivity tomography, SP – self potential) and electromagnetic (i.e. GPR – ground-penetrating radar, GCM – ground conductivity meter) methods are used (Stampolidis et al. 2003, Pilcher et al. 2007, Crocco et al. 2009, 2010, Erasmus 2009, Bimpas et al. 2010, Puust 2010, Demirci et al. 2012, Ayala-Cabrera et al. 2013, 2014, Cataldo et al. 2014, Hadjimitsis et al. 2014, Hawari et al. 2016, Lai et al. 2016, Amran et al. 2018, De Coster et al. 2019, El-Zahab & Zayed 2019, Aslam et al. 2017, 2022, Yang et al. 2022).

In the paper, the author focuses on the most commonly used electromagnetic method applied for the detection of underground water leakages, i.e., the GPR method. The analysis of the literature presented above delivers information that the most often applied technique in the GPR method is the so-called short-offset reflective profiling (SORP) technique and for this technique, all analyses were performed.

In the literature there are many examples of the application of the SORP technique for the detection of water leakages from pipes, where the authors usually used antennae in frequency range between 250–1000 MHz (the highest frequencies were applied during laboratory tests). Some examples present the detection of leakages in real

conditions (Hunaidi & Giamou 1998, Halimshah et al. 2015, Hawari et al. 2016, Cheung & Lai 2019), other in laboratory or in testing sites (Demirci et al. 2012, Ayala-Cabrera et al. 2013, 2014, Lai et al. 2016, Amran et al. 2017, 2018, De Coster et al. 2019, Aslam et al. 2022) and numerical modelling of this problem is also shown in literature (Nakhkash & Mahmood-Zadeh 2004, Crocco et al. 2010, Carrive et al. 2022).

Leakage detection using the SORP technique in homogeneous and isotropic ground, when the surface is not covered by asphalt/concrete, is a simple matter that has been shown and discussed in the literature mentioned above. Detection and monitoring of water leakages in urbanised areas is a much more difficult task and this problem is analysed in this paper on the basis of theoretical and numerical analyses. In towns, the geological medium has been subjected to strong anthropopression in the past and therefore it is always a heterogeneous medium and may also be an anisotropic one; in such ground, a scattering effect often appears and this phenomenon is also discussed in this paper. In urbanised areas, the earth surface is often covered by asphalt, concrete, stone with substructures made of sand/gravel and additional electromagnetic interference often occurs – all these factors were taken into account during the analyses.

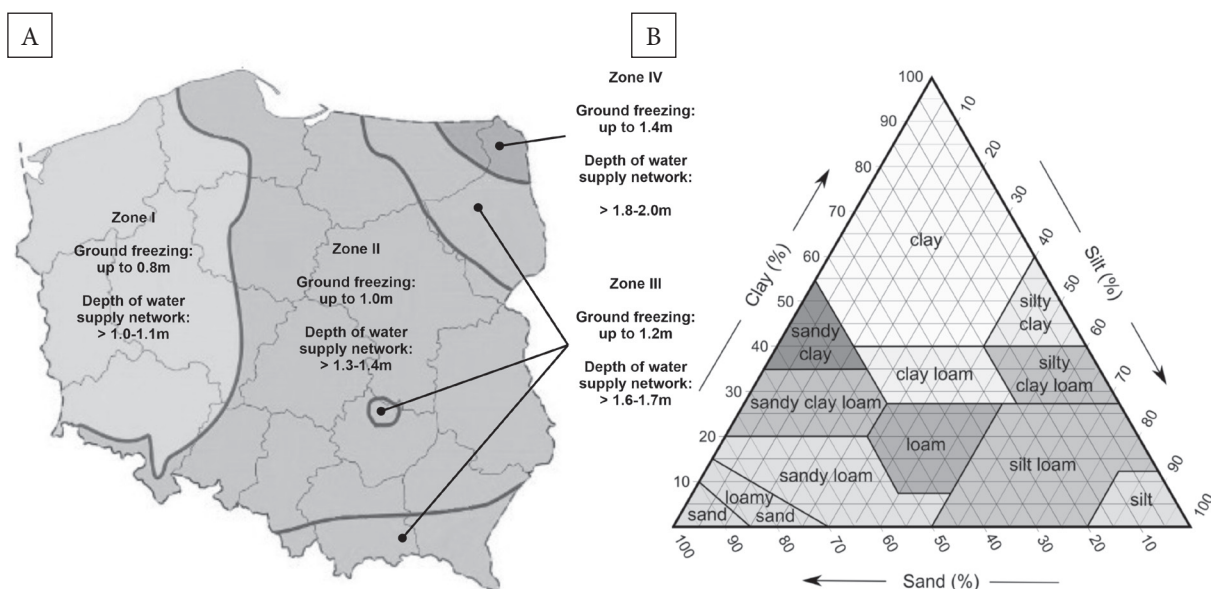


Fig. 1. Depths of the location of water supply networks in Poland (Ustawa... 1994, p. 414) (A); ground classification (PN-EN ISO 14688-1:2006) (B)

## METHODS AND RESULTS

In the first part of this section, the theoretical aspects of the GPR method and the SORP technique are presented.

Among of the GPR devices, different measurement systems are used and different constructions of antennae are implemented. In the further part of the section, the most popular presently GPR construction, i.e., impulse system with bistatic antennae used for 2D surveys carried out from the surface will be described.

In the GPR method, electromagnetic (EM) wave is generated by a transmitter antenna (Tx) and such wave may be presented in form of the TEM (transverse electro-magnetic) wave (Fig. 2A). Transmission of EM wave from typical GPR dipole antenna is shown in Figure 2B, C but for the further analyses a simplified transmission was assumed (Fig. 2D). Propagation of EM wave depends on electromagnetic properties of geological medium, i.e., electrical permittivity  $\varepsilon$  [F/m], magnetic permittivity  $\mu$  [H/m] and electrical conductivity  $\sigma$  [S/m]; in the further analyses, relative permittivity, i.e.,  $\varepsilon_r$  [-] and  $\mu_r$  [-] were taken into account according the Formulae (1) and (2):

$$\varepsilon_r = \frac{\varepsilon}{\varepsilon_0} \quad (1)$$

$$\mu_r = \frac{\mu}{\mu_0} \quad (2)$$

where:

$\varepsilon_r$ ,  $\varepsilon$ ,  $\varepsilon_0$  – adequately relative electrical permittivity [-], electrical permittivity of geological medium [F/m] and electrical permittivity of vacuum [F/m] ( $\varepsilon_0 = 8.85 \cdot 10^{-12}$  F/m),  
 $\mu_r$ ,  $\mu$ ,  $\mu_0$  – adequately relative magnetic permittivity [-], magnetic permittivity of geological medium [H/m] and magnetic permittivity of vacuum [H/m] ( $\mu_0 = 4\pi \cdot 10^{-7}$  H/m).

In the SORP technique, the transmitter (Tx) and receiver (Rx) antennae move along the profile with constant and short offset between Tx and Rx (Fig. 2E); short offset means that the distance between Tx and Rx is less than wave length generated by Tx and some simplifications may be assumed in theoretical analysis. The transmitter antenna emits electromagnetic wave at every specified distance interval ( $\Delta x$ ) and in consequence four kinds

of waves may be distinguished in the geological medium (Fig. 2E), i.e., incident wave (IW), reflected wave (RW), transmitted wave (TW) and direct ground wave (DGW); in the air, additional direct air wave (DAW) and evanescent ground wave (EGW) are created. In the paper, incident and reflected waves in form of the TEM waves will be analysed, because only IW and RW are important in the SORP technique.

The incident wave reflects off underground objects (e.g., from water saturated part of the ground) and geological boundaries (Fig. 3A, B) and propagates back to the surface (Fig. 2E); for the SORP surveys, simplification of reflection presented in Figure 3C is proper and therefore it will be assumed for the further analyses. The contrast of values of  $\varepsilon_r$  in the examined medium decides upon the value of the reflection coefficient  $R$  [-], and in consequence upon the amplitude of the reflections recorded on the radargram. The analyses presented in the further part of the paper will only be conducted for low-loss media, i.e., for media with electrical conductivity  $\sigma \lll 10$  mS/m (assumed that  $\sigma \approx 0$  mS/m); for such media and for simplification presented in Figure 3C reflection coefficient may be described with Formula (3) where assumed that  $\mu_r = 1$  (i.e., non-magnetic medium).

Detailed analysis of the reflection coefficient will be carried out in the “Discussion” section.

$$R = \frac{\sqrt{\varepsilon_{r1}} - \sqrt{\varepsilon_{r2}}}{\sqrt{\varepsilon_{r1}} + \sqrt{\varepsilon_{r2}}} \quad (3)$$

where:

$R$  – reflection coefficient [-],  
 $\varepsilon_{r1}$ ,  $\varepsilon_{r2}$  – adequately relative electrical permittivity of analysed mixture built of sand, silt, clay, and leakage zone [-].

The reflected waves are recorded by the receiver antenna (Rx) and displayed on the computer during the measurement in the form of a radargram. The horizontal axis on the radargram is presented as the distance scale  $x$  [m], whereas the vertical axis is presented as the time scale  $t$  [ns]; during the processing of measured data, the time axis is converted into the depth axis  $z$  [m], taking into consideration the information about the velocity  $v$  [m/ns] of the TEM wave within the studied medium.

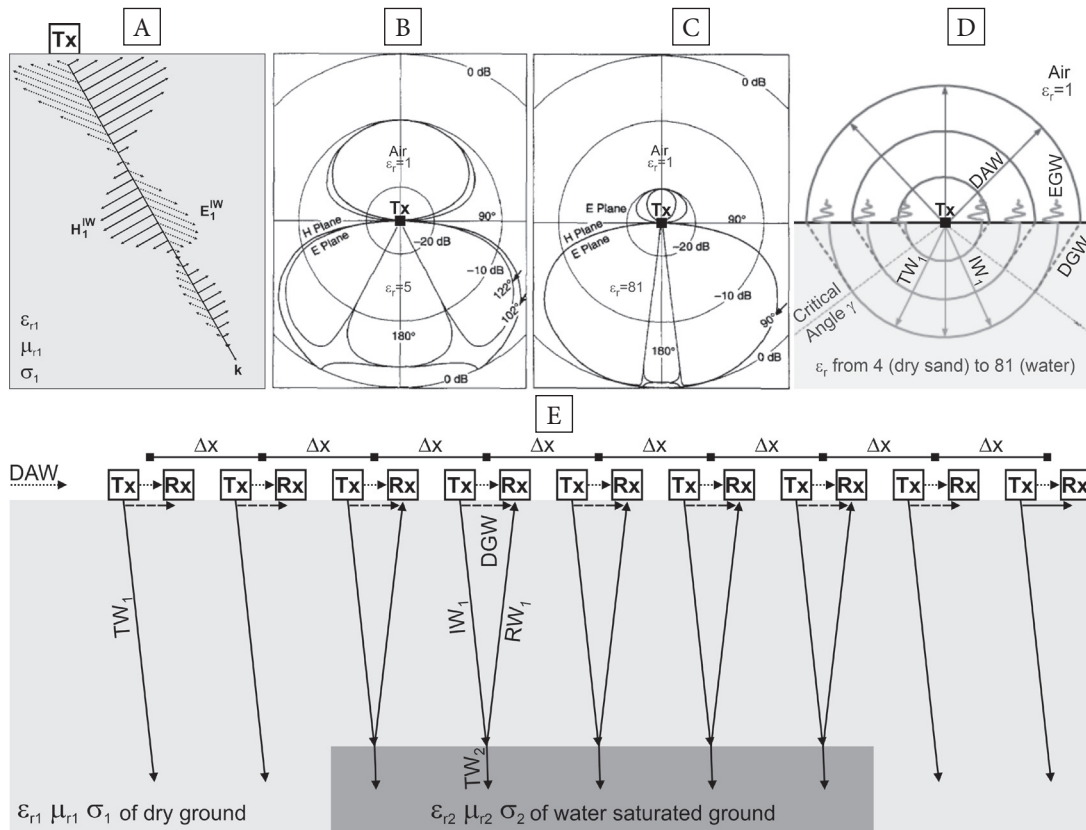


**Fig. 2.** Idea of the TEM wave (A); transverse magnetic TM (H plane) and transverse electric TE (E plane) components of the TEM wave (Arcone 1995) for: medium with  $\epsilon_r = 5$  (dry sand) (B) and medium with  $\epsilon_r = 81$  (water) (C); subsequent positions of different waves' heads for subsequent time steps of analysis (Annan 2001) (D); idea of the SORP surveys (E);  $\gamma$  [deg] – determines a cone contouring of TM and TE components of the TEM wave

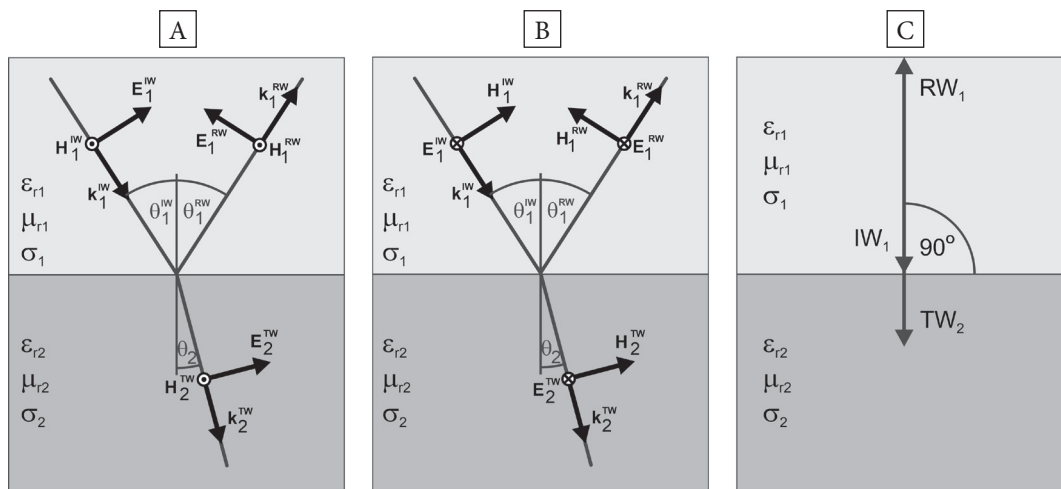


**Fig. 3.** Reflection of TM component of the TEM wave (A); reflection of TE component of the TEM wave (B); simplification of reflection of the TEM wave assumed for further theoretical and numerical analyses, proper for the SORP surveys (C)

To carry out the GPR surveys for different depths and with adequate resolutions, antennae with different frequencies have to be applied. The

typical frequency range of the antennae is between 10 MHz to 1 GHz, but antennae with lower and higher frequencies are used for some specific

surveys. As shown in the “Introduction” section, different authors used antennae in the frequency range between 250–1000 MHz for the detection of water leakages. The highest frequencies were used only during laboratory tests, so the numerical modelling carried out by the author was made for antennae with frequencies of 250 MHz and 500 MHz. The frequency of the antenna defines the resolution of measurements (Table 1), adequately to the simplified Formulae (4)–(7):

$$\Delta r \geq \frac{\lambda}{4} \quad (4)$$

$$\Delta l \geq \sqrt{\frac{\lambda \cdot h}{2}} \quad (5)$$

$$\lambda = \frac{v}{f_c} \quad (6)$$

$$v = \frac{c}{\sqrt{\epsilon_r}} \quad (7)$$

where:

$\Delta r$  – vertical resolution [m],

$\lambda$  – electromagnetic wave length [m],

$\Delta l$  – horizontal resolution [m],

$h$  – depth [m],

$v$  – velocity of electromagnetic wave [m/s],

$f_c$  – central frequency of transmitter antenna [Hz],

$c$  – light velocity [m/s], i.e.,  $3 \cdot 10^8$  m/s.

Vertical and horizontal resolutions as well as depth penetration of the TEM wave (Table 1) are very important information to carry out proper measurements – these issues will be analysed in the “Discussion” section.

The next important matter is velocity of the TEM wave which will also be analysed in the “Discussion” section. For the media analysed in the paper, velocities were calculated on the basis of Formula (7) and presented in Table 2.

Another important matter is the attenuation of the TEM wave. Incident wave, travelling through the ground (Fig. 2E) loses part of its energy due to attenuation, where the attenuation factor  $\alpha_{\text{total}}$  [dB/m] is defined by two components: ohmic attenuation  $\alpha_o$  and scattering attenuation  $\alpha_s$  according to the Formulae (8)–(10). The first component of the attenuation factor i.e., ohmic attenuation calculated for low-loss media from Formula (9) is presented in Table 2.

$$\alpha_{\text{total}} = \alpha_o + \alpha_s \quad (8)$$

$$\alpha_o = 1.69 \cdot 10^3 \frac{\sigma}{\sqrt{\epsilon_r}} \quad (9)$$

$$\alpha_s = \frac{N \xi A_e}{2} \quad (10)$$

where:

$\alpha_{\text{total}}$  – attenuation factor [dB/m],

$\alpha_o$  – ohmic attenuation [dB/m],

$\alpha_s$  – scattering attenuation [dB/m],

$N$  – number of scatterers per  $1 \text{ m}^3$ ,

$\xi$  – fraction of power which is reemitted by everyone scatterers [W],

$A_e$  – effective cross-section of everyone scatterers [ $\text{m}^2$ ].

To date, the analysis of scattering effects and scattering attenuation has only been tackled in the geophysical literature relatively rarely (Radzevicius & Daniels 2000, Annan 2001, Muller 2005, Grimm et al. 2006, Al-Qadi et al. 2008, Ying et al. 2019, Ponti et al. 2020). In practice, the attenuation factor is usually described only by ohmic attenuation and scattering attenuation is omitted in analysis; this is due to the fact that it is very difficult to properly describe the unique distribution of scatterers, their properties, dimensions etc.

**Table 1**

Basic parameters of the GPR antennae usually used for water leakage detection (on the basis of literature presented in the “Introduction” section)

Central frequency of antennae $f_c$ [MHz]	Vertical resolution $\Delta r$ [m] in typical ground where $\epsilon_r = 9$	Horizontal resolution $\Delta l$ [m] in typical ground where $\epsilon_r = 9$	Max. depth range $h_{\text{max}}$ [m] in lossless media*
250	0.10	0.45 at $h = 1$ m 0.63 at $h = 2$ m	10.0
500	0.05	0.32 at $h = 1$ m 0.45 at $h = 2$ m	5.0
1000	0.02	0.22 at $h = 1$ m 0.32 at $h = 2$ m	1.5

\* Information from materials delivered by the firm Guidelinegeo (www.guidelinegeo.com).

**Table 2**

Mean values of material properties for media analysed in the paper on the basis of Plewa & Plewa (1992), Annan (2001), Saarenketo (2003), Porubiaková & Komačka (2015), and Wutke et al. (2019)

Medium*	Relative electrical permittivity $\epsilon_r$ , [-]	Relative magnetic permittivity $\mu_r$ , [-]	Electrical conductivity $\sigma$ [mS/m]	Velocity of TEM wave $v$ [m/ns]	Ohmic attenuation factor $\alpha_o$ [dB/m]
Dry – water saturated sand	4–30	1	0.01–1	0.15–0.06	0.01–1
Dry – water saturated silt	5–30	1	1–100	0.13–0.06	1–100
Dry – water saturated clay	5–40	1	1–1000	0.13–0.05	1–300
Dry mixture (built of sand, silt, clay)	9	1	1	0.10	1
Water saturated mixture (built of sand, silt, clay)	30	1	10**	0.06	10
Void filled with water	81	1	0.5	0.03	0.1
Suffosion zone filled with air	1	1	0	0.30	0
Concrete/asphalt	6	1	0.01	0.12	0.01
Substructure (dry compacted sand)	4	1	0.01	0.15	0.01
Scatterers – stone, asphalt, concrete, ceramic	4–9	1	0.01–1	0.15–0.10	0.01–1

\* With grey colour marked values assumed for numerical modelling.

\*\* Max. values of conductivity of water saturated media are  $10^2$ – $10^3$  mS/m; for the GPR method conductivity equals ca. 10 mS/m is max. value above which surveys have no sense due to high ohmic attenuation – therefore for numerical modelling  $\sigma = 10$  mS/m was assumed.

In urbanised areas, where different scatterers often occur in the ground, scattering attenuation plays a more important role than ohmic attenuation. To illustrate the magnitude of scattering attenuation, a simplified Formula (11) was used to count values of  $\alpha_s$  (Fig. 4). Example calculations were carried out for spherical metallic scatterers ( $\epsilon_r = 1$ ) with diameters  $a$  equals 0.1 m and 0.25 m, located in dry and water saturated mixture of sand, silt, clay – adequate value of  $\epsilon_r$  of mixture was taken from Table 2. Analysis was carried out for volume of  $1 \text{ m}^3$  with regularly distributed in space metallic spheres with different their numbers  $N$ , i.e.,  $N = 64$  and  $N = 125$ .

$$\alpha_s = \epsilon_r^2 N a^6 f_c^4 \cdot 10^{-6} \quad (11)$$

The analysis of the information presented in Figure 4 allows a general conclusion to be drawn that scattering attenuation does not have an important influence on the TEM wave with frequencies below 100 MHz. As mentioned before, antennae with frequencies 250, 500, 1000 MHz (Table 1)

are usually applied for water leakage detection and then scattering attenuation should be taken into account (see Fig. 4), especially in urbanised areas where scatterers often occur.

The comparison of the values of ohmic attenuation (Table 2) and scattering attenuation (Fig. 4) shows that in the analysed situations, values of  $\alpha_o$  vary from 0 to  $10^2$  whereas values of  $\alpha_s$  vary from  $10^1$  to  $10^7$ ; therefore, the analysis of scattering attenuation is more important than the analysis of ohmic attenuation and such an analysis will be carried out in the further part of this section using numerical modelling.

In the second part of this section, numerical modelling will be performed, based on the theoretical aspects presented above. Numerical simulations were carried out for simplifications and assumptions described in the earlier part of this section.

The most popular technique for modelling of electromagnetic wave field for the GPR method is the FDTD (finite difference time domain) technique (Yee 1966, Fomberg 2003, Gołębowski 2004, 2006, 2015).

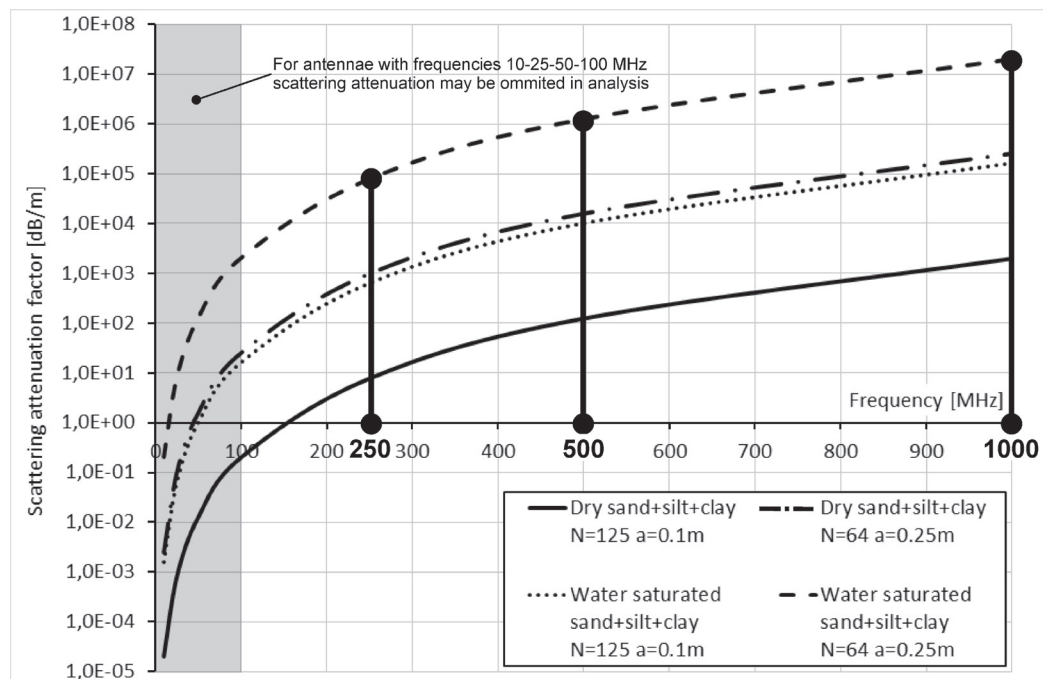


Fig. 4. Values of scattering attenuation factor  $\alpha_s$  for media analysed in the paper; water saturated mixture of sand, silt, clay refers to leakage zone

Numerical modelling was carried out in 3D mode with the use of module Modelling (based on the FDTD technique) of computer program ReflexW, ver. 10, licence number 1288 (www.sandmeier-geo.de).

In a discrete model (Fig. 5) material properties (Table 2) were defined in the grid points and the components of the electromagnetic wave field were also only solved in the grid points.

In all models, 2" metal water pipes were inserted – material properties of pipes were as follow:  $\epsilon_r = 1$ ,  $\mu_r = 1$ ,  $\sigma = 100$  S/m.

On the upper boundary of numerical models, a strip with the material properties of air was introduced; on the other boundaries, absorbing boundary condition was applied (Fig. 5).

For excitation of propagation of the TEM wave in the models, sources with frequencies 250 MHz and 500 MHz were defined; sources as well as registration points were defined as shown in Figure 5.

Solving was carried out in time window  $T = 100$  ns with time steps  $\Delta t = 0.01$  ns. Simulations were carried out for three scenarios (Figs. 6A–9A): 1) water leaks very slowly from a damaged pipe and fully fills a porous space in the ground and

- process of suffosion is not observed – part of the model called “Water saturated mixture”;
- 2) water leaks very intensively from a damaged pipe and water destroys the ground and process of suffosion is observed – part of the model called “Void filled with water”;
  - 3) an underground hole was created by suffosion and water flowed in deeper parts of the ground and the hole is filled with air – part of model called “Suffosion zone filled with air”.

For all of the mentioned situations, additional noise was applied during the modelling which is typical for the GPR surveys conducted in urbanised areas and simulates interferences:

- noise with amplitude equals 10% of max. amplitude of source signal and frequencies adequate 500 MHz and 250 MHz – figures with signature B;
- noise with amplitude equals 25% of max. amplitude of source signal and frequencies adequate 500 MHz and 250 MHz – figures with signature C;
- noise with amplitude equals 50% of max. amplitude of source signal and frequencies adequate 500 MHz and 250 MHz – figures with signature D.

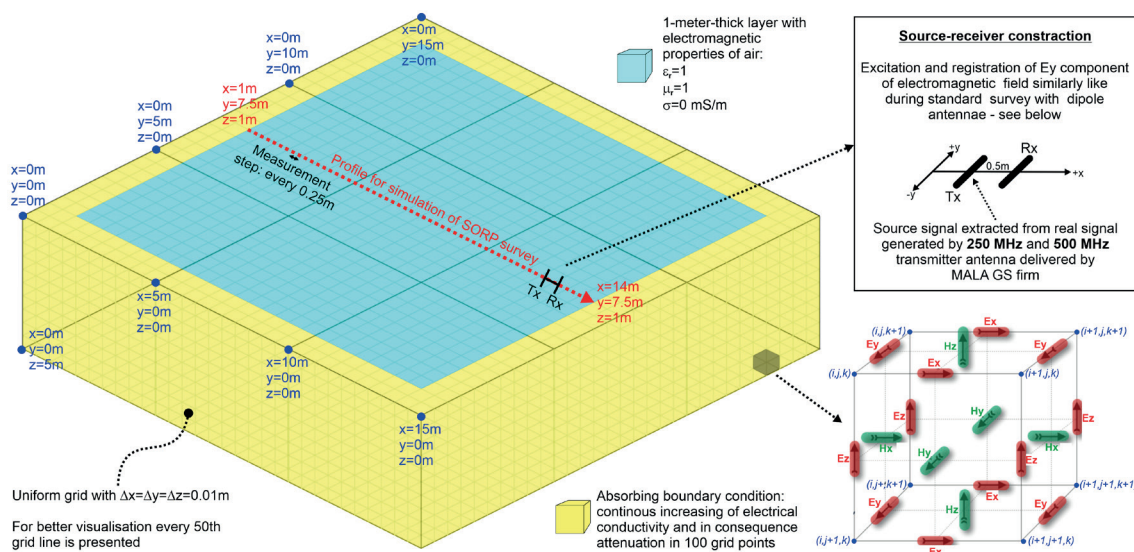


Fig. 5. Outer view of numerical model constructed for analysis of water leakages into the ground

The most difficult stage of preparing the models was the proper construction of the ground with scatterers for the simulation of the geological medium which occurs in urbanised areas, where many anthropogenic objects often appear. Usually, it is impossible to describe the dimensions of several scatterers and their distribution in space, impeding the reproduction of the detailed material properties of a medium built of sand, silt, clay, and scatterers. In such situations, the only construction technique for such a medium in a numerical model seems to be via the application of a stochastic model. A detailed description of the application of stochastic model in the interpretation of the GPR data was presented in publications by Gołębowski (2012, 2015) but only the fundamental information is presented in the next paragraph.

At the first step of preparing the models, the material properties (i.e.,  $\epsilon_r$ ,  $\mu_r$ ,  $\sigma$ ) for a dry mixture of sand, silt, clay (from Table 2) were introduced to the numerical models. As the second step, a random generator was applied for random location of scatterers in the analysed mixture; for this step, adequate addresses  $i$ ,  $j$ ,  $k$  of grid points were randomly chosen; then, for every randomly chosen grid point, randomly generate values of  $\epsilon_r$  and  $\sigma$  of debris consists of stone, asphalt, concrete, ceramic were prescribed – values were chosen from periods:

$\epsilon_r = 4-9$  and  $\sigma = 0.01-1$  mS/m (Table 2). During the simulations, a constant value  $\mu_r = 1$  was assumed since non-magnetic media were analysed.

The results of the modelling are shown in the following figures:

- Fig. 6 – synthetic radargrams for a model of an isotropic and homogenous mixture build of sand, silt, clay and 500 MHz source,
- Fig. 7 – synthetic radargrams for a model of a mixture with small (dimension  $0.1 \text{ m} \times 0.1 \text{ m}$ ) scatterers and 500 MHz source,
- Fig. 8 – synthetic radargrams for a model of a mixture with small (dimension  $0.1 \text{ m} \times 0.1 \text{ m}$ ) scatterers and 250 MHz source,
- Fig. 9 – synthetic radargrams for a model of a mixture with bigger (dimension  $0.25 \text{ m} \times 0.25 \text{ m}$ ) scatterers and 250 MHz source.

Amplitudes in synthetic radargrams (graphs B, C, and D in Figures 6–9) were presented in normalised form with normalisation to the max. amplitude of the source signals.

Numerical simulations were conducted for both antennae and for locations of water pipes in different depths, between 1–2 m (Fig. 1A); additionally different dimensions of scatterers and different shapes of leakage zones were analysed. In Figures 6–9 only the most interesting results are presented since they seem sufficient to draw some general conclusions.

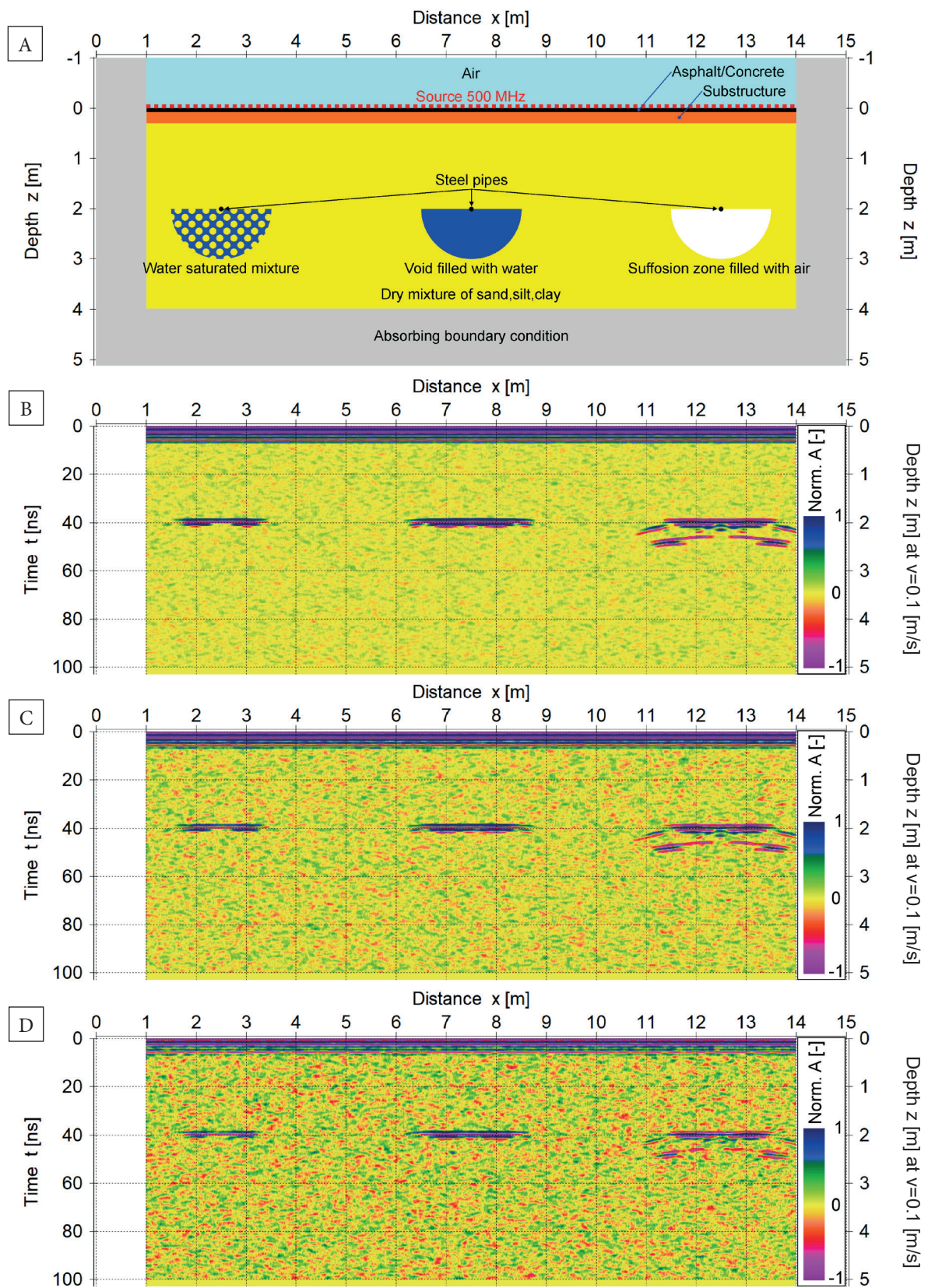


**Fig. 6.** Cross-section of numerical model from Figure 5 at  $y = 7.5$  m: A) model of isotropic and homogenous mixture with water pipes located at depth of 2.0 m (Zone IV, Fig. 1A) and 500 MHz source; B) synthetic radargram with noise equals 10%; C) synthetic radargram with noise equals 25%; D) synthetic radargram with noise equals 50%

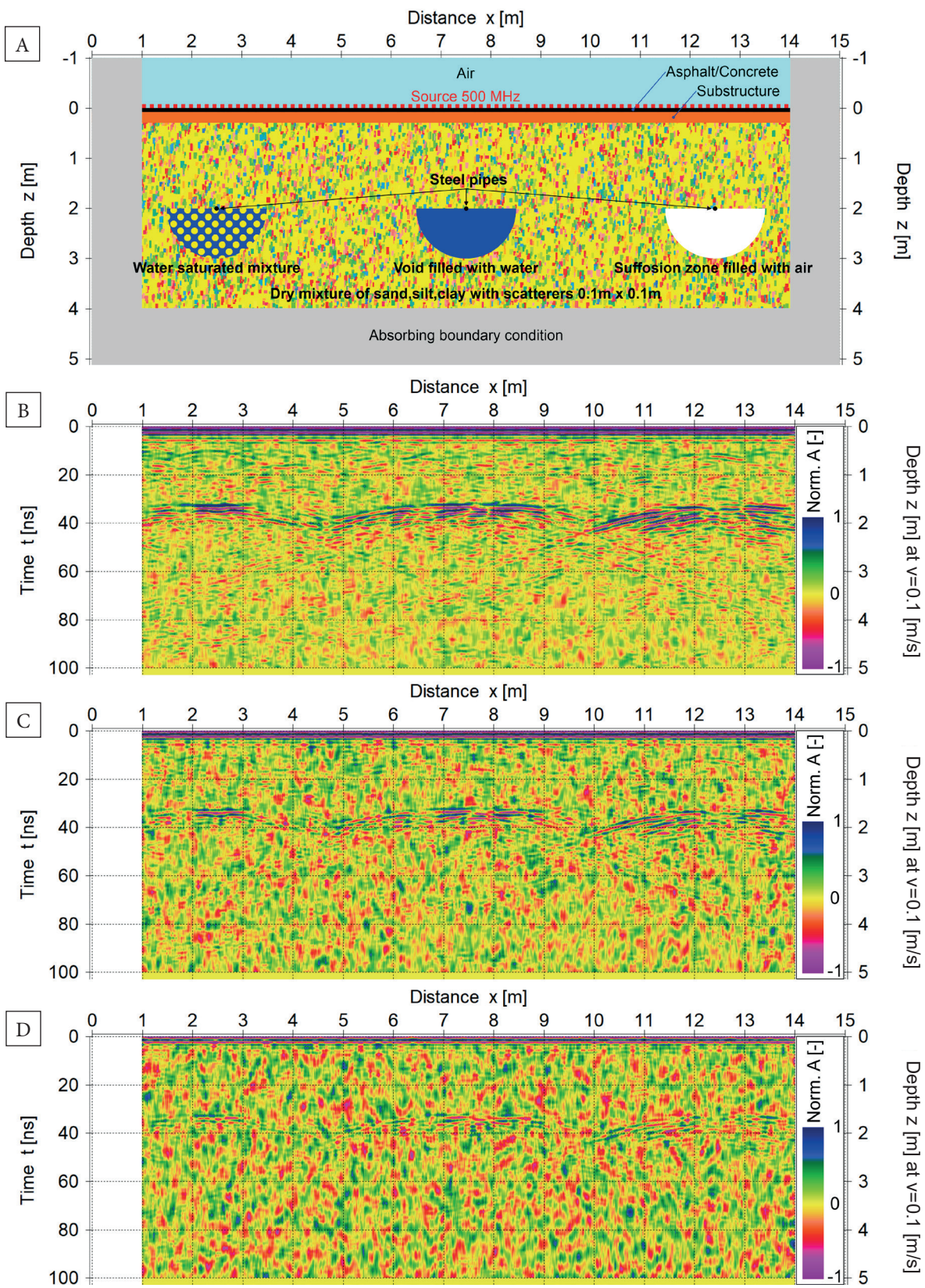
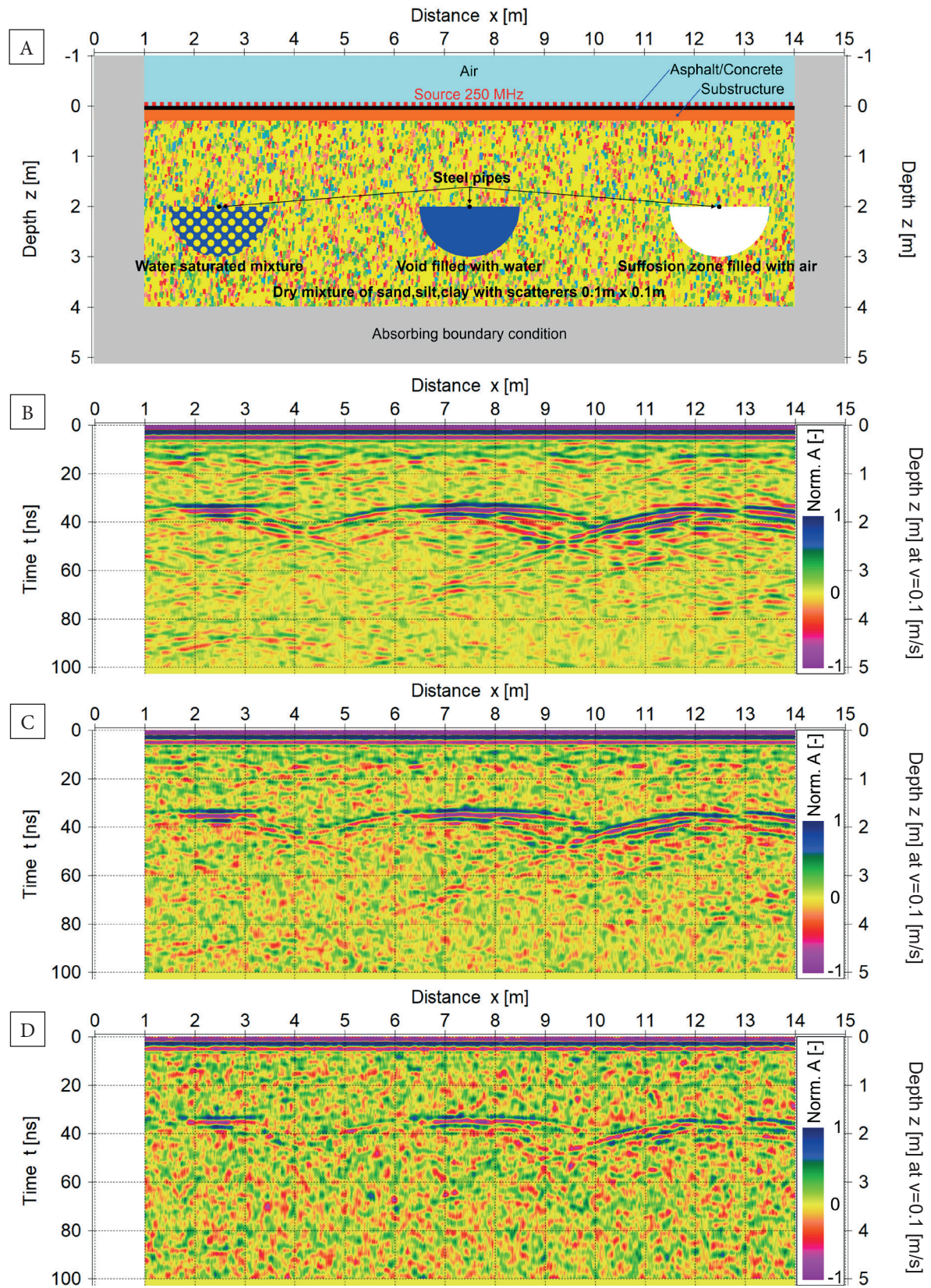
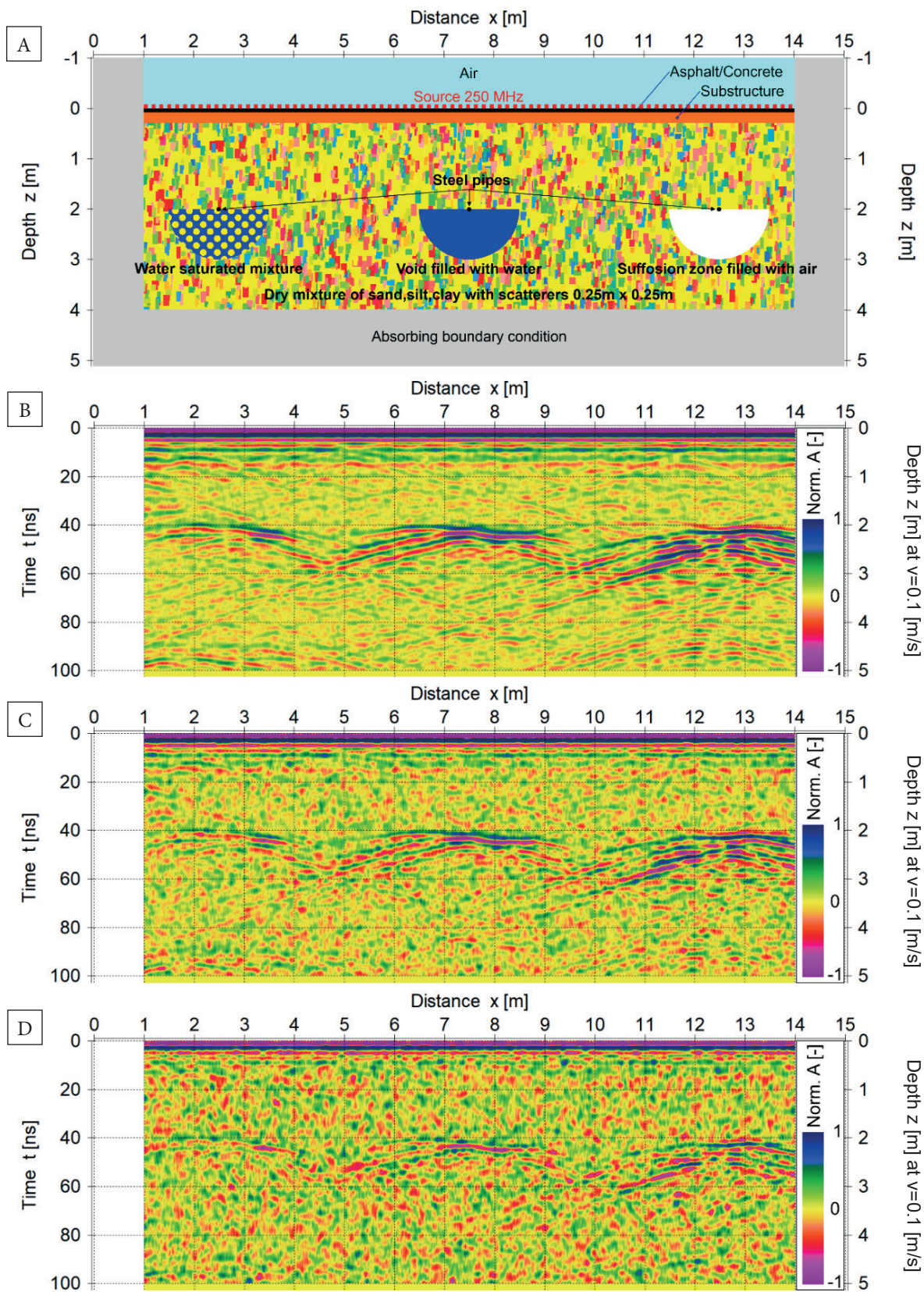


Fig. 7. Cross-section of numerical model from Figure 5 at  $y = 7.5$  m: A) model of mixture with small scatterers ( $0.1\text{ m} \times 0.1\text{ m}$ ) and water pipes located at depth of 2.0 m (Zones IV, Fig. 1A) and 500 MHz source; B) synthetic radargram with noise equals 10%; C) synthetic radargram with noise equals 25%; D) synthetic radargram with noise equals 50%



**Fig. 8.** Cross-section of numerical model from Figure 5 at  $y = 7.5$  m: A) model of mixture with small scatterers ( $0.1\text{ m} \times 0.1\text{ m}$ ) and water pipes located at depth of 2.0 m (Zones IV, Fig. 1A) and 250 MHz source; B) synthetic radargram with noise equals 10%; C) synthetic radargram with noise equals 25%; D) synthetic radargram with noise equals 50%



**Fig. 9.** Cross-section of numerical model from Figure 5 at  $y = 7.5$  m: A) model of mixture with bigger scatterers ( $0.25\text{ m} \times 0.25\text{ m}$ ) and water pipes located at depth of 2.0 m (Zones IV, Fig. 1A) and 250 MHz source; B) synthetic radargram with noise equals 10%; C) synthetic radargram with noise equals 25%; D) synthetic radargram with noise equals 50%

## DISCUSSION

In this section, five factors important for the SORP surveys will be analysed, i.e., reflection coefficient, polarity of reflections, resolution, velocity, and attenuation of the TEM wave.

### Reflection coefficient

For all of the situations analysed in the paper, reflection coefficients  $R$  were counted on the basis of Formula (3) and information from Table 2 and were presented in Table 3.

At the beginning, reduction of source signal energy caused by the reflection of the TEM wave from the boundary between the pavement (i.e., asphalt/concrete) and the substructure (i.e., dry compacted sand) as well as between the substructure and the dry mixture (built of sand, silt, clay) should be analysed. Values of  $R$  for both boundaries are low (Table 3), so only a small fraction of signal energy is reflected back and most of the energy is transmitted into the ground; as a result, these boundaries should not be disturbed during surveys.

**Table 3**

Values of reflection coefficients  $R$  [-] for media analysed in the paper

Media	$R^*$ [-]
Dry mixture ( $\epsilon_r = 9$ ) and water saturated mixture ( $\epsilon_r = 30$ )	-0.3
Dry mixture ( $\epsilon_r = 9$ ) and void filled with water ( $\epsilon_r = 81$ )	-0.5
Dry mixture ( $\epsilon_r = 9$ ) and suffosion zone filled with air ( $\epsilon_r = 1$ )	0.5
Pavement ( $\epsilon_r = 6$ ) and substructure ( $\epsilon_r = 4$ )	0.1
Substructure ( $\epsilon_r = 4$ ) and dry mixture ( $\epsilon_r = 9$ )	-0.2

\* Positive and negative values denote polarity of reflections.

The results of theoretical analysis (Table 3) and numerical modelling (Fig. 6B–D) for isotropic and homogenous dry mixture deliver information that the detection of water leakage from pipe located between depths of 1.0–2.0 m (see Fig. 1A) is a simple matter; similar conclusion may be found in literature cited in the “Introduction” section. The appearance of low (Fig. 6B), medium (Fig. 6C) and high interferences (Fig. 6D) during the surveys should not prevent their

proper interpretation, because the high value of  $R$  (Table 3) allows high-amplitude reflections to be recorded on radargrams. In all three cases analysed in the paper, there is no possibility to outline anomalous zones but only reflections from the top of these zones may be recorded and interpreted; this fact constitutes a limitation of the GPR method for leakage detection. It should be noted, that in real conditions, some level of heterogeneity always occurs in the ground and anisotropy is often observed during GPR surveys; in such real conditions, unambiguous interpretation of leakages at greater depths (i.e., >2.0 m) in the urbanised areas (where interference often occur) may be difficult, especially for the situation called “water saturated ground” (Fig. 6D).

Analysis of reflection coefficients for a mixture of sand, silt, clay with scatterers will be carried out together with the analysis of attenuation in the “Attenuation of the TEM wave” sub-section.

### Polarity of reflection

The polarity of reflections recorded in radargrams (positive and negative values in Table 3) may be a useful interpretation tool only for simple geological situations; in such situations, change of polarity of several reflections compared to the polarity of the source signal allows the proper interpretation of material filling of void/porous space. For example, void filled with water and air both have the same values of  $R$  but have the opposite polarity (see Table 3, Fig. 6B–D). Unfortunately, in the cases analysed in this paper, the presence of scatterers with different material properties precludes the use of the polarity of reflections during interpretation, but in some simple situations (e.g., Fig. 6B) this factor should be taken into account.

### Resolution

Horizontal and vertical resolutions of the GPR method which are a function of wave length (which follows from antenna frequency) and the velocity of the TEM wave are not constant values (Table 1). Numerical simulations were carried out for leakage zones with different shapes and dimensions; the shapes did not significantly influence the possibility of leakage detection but the dimensions strongly influenced the results. After simulation of precipitation during modelling, the

resolution was higher in the wet medium than in the dry one, which explains Formulae (4)–(7). In the wet medium, the detection of small suffosion zones is easier than in the dry one but it should be stressed that the reflection coefficient between wet medium and water-saturated zone is lower and it makes difficult to detect leakages. Usually, a leakage is large, so resolution is not as important as the value of the reflection coefficient and therefore it is better to carry out the GPR surveys in dry ground where the resolution of measurements is lower (see Table 1).

### Velocity of the TEM wave

Velocity may be a factor used to distinguish the material (in analysed situations, water and air) filling the void/porous space of the ground. Taking into account velocity during interpretation is done by the analysis of the position of the geological boundary (or known anthropogenic object) recorded below the leakage zone. In the suffosion zone filled with air (Fig. 6–9A) the velocity of the TEM wave equals 0.3 m/ns but in water-saturated mixture and in void filled with water (Fig. 6–9A) the velocities are similar and vary between 0.03–0.06 m/ns (Table 2). This difference in velocities means that reflections from a boundary/object located below a leakage appear in the radargram for a lower time for air-saturated region and a greater time for water-saturated areas; in consequence, an apparent curvature of horizontal geological boundary may be an indicator which can deliver information about whether the ground around a pipe is dry (suffosion zone filled with air) or wet (ground filled with water).

### Attenuation of the TEM wave

A dry mixture of sand, silt, and clay has a higher value of ohmic attenuation  $\alpha_o$  (Table 2) than typical sandy ground but the value of  $\alpha_o$  of dry mixture does not strongly influence the possibility of detection.

After precipitation, ohmic attenuation will reach high values in the analysed mixture (Table 2) and detection will be impossible. The presence of water in the ground surrounding a leakage zone also reduces the contrast of material properties between wet ground and the leakage area which was discussed in the “Reflection coefficient” sub-section.

If the heterogeneity of ground appears in the form of scatterers located in the geological medium, detection of leakages at depths between 1.0–2.0 m (Fig. 1A) only seems to be possible for low level of interferences (Fig. 7B); the possibility of leakage detection results from the fact that reflection coefficients for three analysed scenarios of leakages are sufficiently high compared to the effects on radargram caused by scattering and interference.

For medium and high interferences (Fig. 7C, D), location of leakages is rather impossible due to the fact that high amplitudes of reflections on radargrams are caused by scattering effects and interference rather than by the value of the reflection coefficient in leakage zones.

The solution to the detection problem presented in Figures 7C, D may be the application of antennae with lower frequencies which are less susceptible to scattering attenuation (Fig. 4) and, due to their lower resolution (Table 1), they are not as sensitive to small scatterers. The numerical simulation carried out for a source with a lower frequency, i.e., 250 MHz confirms the presented assumption; for leakage which may appear relatively deep, i.e. at depth of 2 m, for all scenarios analysed in the paper, readable reflections are noticed for low and medium level of interferences due to the sufficiently high values of reflection coefficient (Fig. 8B, C); it may be assumed that for high interferences, the proper location of the leakage zone will be difficult (Fig. 8D).

The application of antennae with a lower frequency, e.g., 250 MHz, may solve the interpretation problem even when bigger scatterers occur in the ground but a limitation will be the level of interference (Fig. 9B–D). When in the examined ground, bigger scatterers occur and level of interferences is medium and high, the detection of effects caused by leakages is impossible, especially for the situation known as “water saturated ground” (Fig. 9C, D) which appears the most often in reality. This is due to the fact that amplitudes of reflections on radargrams resulting from the reflection coefficient in leakage zones are too low in comparison to amplitudes generated by scattering effects and interferences.

Successive lowering of the antennae frequency might theoretically solve the problem of scattering

attenuation (Fig. 4) but antennae with frequencies lower than 100 MHz have very low resolutions and cannot detect small leakages and voids. Additionally, low-frequency antennae are not shielded and the interference which often occurs in urbanised areas may make any interpretation impossible.

Numerical modelling is a certain simplification of real conditions and this was presented and discussed in the theoretical part of the paper; therefore, not all of the relevant aspects may be analysed during simulations. The results of the theoretical and numerical analyses should be regarded as supplying qualitative information but general conclusions may be drawn on the basis of the results presented.

## CONCLUSION

On the basis of the theoretical analysis and numerical simulations presented in this paper, the GPR detection of leakages from water supply networks in urbanised areas is far from an easy matter. Two main problems which appear in such areas are: (a) interferences which always occur but have different levels and (b) presence of different scatterers in the geological medium which cause the scattering attenuation of electromagnetic wave. Occasionally, an additional problem will be large amounts of clay in the ground which increases the ohmic attenuation.

Water supply networks in Poland are located between depths of 1–2 m (in other countries these are similar depths), so antennae with frequency of 500 MHz seem to be the most suitable for terrain surveys; for specific situations, antennae with higher or lower frequencies may be used. The analyses presented in the paper were carried out for ground which was a mixture of sand, silt, and clay; such a mixture may be treated as typical reference ground.

As demonstrated in the paper, if leakages appear in isotropic and homogenous medium of typical ground, the detection of leakage zones is possible even when the interference level is relatively high. This assumption was confirmed by the results of numerical modelling performed for 500 MHz antennae. The maximum level of interferences assumed during the simulations was 50% of the amplitude of the transmitted signal. It is

obvious that for amplitudes of interference higher than 50%, the detection possibility decreases. General conclusions which may be drawn for isotropic and homogenous typical ground are: (i) leakage detection is possible in dry ground with small amounts of clay; the detection possibility strongly decreases in wet ground due to the increase in ohmic attenuation; (ii) if the level of interference is lower than 50%, leakage detection should be possible; (iii) resolution of the GPR method increases in wet ground but the reflection coefficient between wet ground and the leakage zone decreases in such a medium, making leakage detection more difficult. All these conclusions are also valid for typical ground with scatterers.

When leakages appear in a medium with scatterers, and such media are typical for the urbanised areas, detection of leakages becomes a more difficult task. Small scatterers, with dimensions similar to the resolution of selected antennae, influence to some extent the increase in the scattering attenuation. If the dimensions of scatterers are larger than the resolution of the antennae, scattering attenuation can make interpretation more difficult or even impossible. It has to be noted that both ohmic and scattering attenuations increase after precipitation in wet ground, and the detection of leakage zones may be impossible. In areas where scatterers occur, the detection potential of the GPR method may be increased by the application of antennae with lower frequency, e.g., 250 MHz, but the resolution of the surveys will suffer.

As scatters often occur in urbanised areas, with additional interferences with low (ca. 10%) and medium (ca. 25%) amplitudes appearing, this may make interpretation difficult and ambiguous. Among the three analysed cases, i.e., water saturated ground, void filled with water and void filled with air, the most difficult for GPR detection is the first and which in reality appears the most frequently.

If both scatterers and high interferences (greater than 50%) occur in the measurement sites, detection of leakages using of 250 and 500 MHz antennae is very difficult or even impossible; a solution to this problem seems to be application of low-frequency shielded antennae, e.g., 100 MHz; the application of such antennae allows only large leakages to be detected.

In the paper, theoretical and numerical analyses were carried out for typical ground and for selected scenarios of water leakages into the ground; also, selected type of interferences and scatterers were analysed. Such assumptions allowed the general conclusions presented above to be drawn. Further laboratory tests and terrain surveys for different ground types where scattering effects are observed and different interferences may occur are needed for confirmation/modification of the theoretical and numerical analyses presented in the paper.

*The paper was financed by a research grant from the Department of Geoengineering and Water Management, Faculty of Environmental Engineering and Energy, Cracow University of Technology.*

## REFERENCES

- Al-Qadi I.L., Xie W. & Roberts R., 2008. Scattering analysis of ground-penetrating radar data to quantify railroad ballast contamination. *NDT & E International*, 41(6), 441–447. <https://doi.org/10.1016/j.ndteint.2008.03.004>.
- Amran T.S.T., Ismail M.P., Ahmad M.R., Amin M.S.M., Sani S. & Azreen N., 2017. Detection of underground water distribution piping system and leakages using Ground Penetrating Radar (GPR). *AIP Conference Proceedings*, 1799, 030004. <https://doi.org/10.1063/1.4972914>.
- Amran T.S.T., Ismail M.P., Ahmad M.R. & Amin M.S.M., 2018. Monitoring underground water leakage pattern by ground penetrating radar (GPR) using 800 MHz antenna frequency. *IOP Conference Series: Materials Science and Engineering*, 298, 012002. <https://doi.org/10.1088/1757-899X/298/1/012002>.
- Annan A.P., 2001. *Ground Penetrating Radar – workshop notes*. Sensor and Software Inc., Ontario, Canada.
- Arcone S.A., 1995. Numerical studies of the radiation patterns of resistively loaded dipoles. *Journal of Applied Geophysics*, 33, 39–52. [https://doi.org/10.1016/0926-9851\(95\)90028-4](https://doi.org/10.1016/0926-9851(95)90028-4).
- Aslam H., Kaur M., Sasi S., Mortula M., Yehia S. & Ali T., 2017. A conceptual approach to detection of water pipe leakage using non-destructive techniques. [in:] *Proceedings of the 5<sup>th</sup> International Conference on Water, Energy and Environment, Sharjah, United Arab Emirates*, 28.02–2.03.2017, 1–12.
- Aslam H., Mortula M.M., Yehia S., Ali T. & Kaur M., 2022. Evaluation of the factors impacting the water pipe leak detection ability of GPR, infrared cameras, and spectrometers under controlled conditions. *Applied Sciences*, 12(3), 1683. <https://doi.org/10.3390/app12031683>.
- Ayala-Cabrera D., Herrera M., Izquierdo J., Ocaña-Levario S.J. & Pérez-García R., 2013. GPR-based water leak models in water distribution systems. *Sensors*, 13(12), 15912–15936. <https://doi.org/10.3390/s131215912>.
- Ayala-Cabrera D., Campbell E., Carreño-Alvarado E.P., Izquierdo J. & Pérez-García R., 2014. Water leakage evolution based on GPR interpretations. *Procedia Engineering*, 89, 304–310. <https://doi.org/10.1016/j.proeng.2014.11.192>.
- Bimpas M., Amditis A. & Uzunoglu N., 2010. Detection of water leaks in supply pipes using continuous wave sensor operating at 2.45 GHz. *Journal of Applied Geophysics*, 70(3), 226–236. <https://doi.org/10.1016/j.jappgeo.2010.01.003>.
- Carrive P., Saintenoy A., Leger E., Arcone S.A. & Sailhac P., 2022. Exploiting ground-penetrating radar signal enhancements by water-saturated bulb surrounding defective waterpipes for leak detection. *Geosciences*, 12(10), 368. <https://doi.org/10.3390/geosciences12100368>.
- Cataldo A., Persico R., Leucci G., Benedetto E., Cannazza G., Matera L. & Giorgi L., 2014. Time domain reflectometry, ground penetrating radar and electrical resistivity tomography: A comparative analysis of alternative approaches for leak detection in underground pipes. *NDT & E International*, 62, 14–28. <https://doi.org/10.1016/j.ndteint.2013.10.007>.
- Cheung B.W.Y. & Lai W.W.L., 2019. Field validation of water-pipe leakage detection through spatial and time-lapse analysis of GPR wave velocity. *Near Surface Geophysics*, 17(3), 231–246. <https://doi.org/10.1002/nsg.12041>.
- Crocco L., Prisco G., Soldovieri F. & Cassidy N.J., 2009. Early-stage leaking pipes GPR monitoring via microwave tomographic inversion. *Journal of Applied Geophysics*, 67(4), 270–277. <https://doi.org/10.1016/j.jappgeo.2008.09.006>.
- Crocco L., Soldovieri F., Millington T. & Cassidy N.J., 2010. Bistatic tomographic GPR imaging for incipient pipeline leakage evaluation. *Progress in Electromagnetics Research*, 101, 307–321. <https://doi.org/10.2528/PIER09122206>.
- De Coster A., Pérez Medina J.L., Nottebaere M., Alkhalifeh K., Neyt X., Vanderdonck J. & Lambot S., 2019. Towards an improvement of GPR-based detection of pipes and leaks in water distribution networks. *Journal of Applied Geophysics*, 162, 138–151. <https://doi.org/10.1016/j.jappgeo.2019.02.001>.
- Demirci S., Yigit E., Eskidemiir I.H. & Ozdemir C., 2012. Ground penetrating radar imaging of water leaks from buried pipes based on back-projection method. *NDT & E International*, 47, 35–42. <https://doi.org/10.1016/j.ndteint.2011.12.008>.
- El-Zahab S. & Zayed T., 2019. Leak detection in water distribution networks: An introductory overview. *Smart Water*, 4, 5. <https://doi.org/10.1186/s40713-019-0017-x>.
- Erasmus V.M., 2009. *Methods of pipe and leak detection in underground water and sewer reticulations*. University of Pretoria [B.Sc. dissertation].
- Fomberg B., 2003. Some numerical techniques for Maxwell's equations in different types of geometries. [in:] Ainsworth M., Davies P., Duncan D., Rynne B. & Martin P. (eds.), *Topics in Computational Wave Propagation: Direct and Inverse Problems*, Lecture Notes in Computational Science and Engineering, 31, Springer, Berlin, Heidelberg, 265–299. [https://doi.org/10.1007/978-3-642-55483-4\\_7](https://doi.org/10.1007/978-3-642-55483-4_7).

- Gołębowski T., 2004. Wprowadzenie do metodyki interpretacji badań georadarowych przy użyciu procedury modelowania numerycznego [Introduction to interpretation of GPR data using of numerical modelling]. *Przeegląd Geologiczny*, 52(7), 563–568.
- Gołębowski T., 2006. Numeryczne modelowanie pola georadarowego przy pomocy metody FDTD [Numerical modeling of GPR wave field using of FDTD technique]. *Geoinformatica Polonica*, 8, 23–36.
- Gołębowski T., 2012. *Zastosowanie metody georadarowej do detekcji i monitoringu obiektów o stochastycznym rozkładzie w osrodku geologicznym* [Application of the GPR method for detection and monitoring of objects with stochastic distribution in the geological medium]. Rozprawy, Monografie – Akademia Górniczo-Hutnicza im. Stanisława Staszica, 251, Wydawnictwa AGH, Kraków.
- Gołębowski T., 2015. Introduction to numerical modeling of electromagnetic wave field on the example of georadar data recorded in river dike. *Technical Transactions – Environmental Engineering*, 112(2-Ś), 39–53. <https://doi.org/10.4467/2353737XCT.15.225.4611>.
- Grimm R.E., Heggy E., Clifford S., Dinwiddie C., McGinnis R. & Farrell D., 2006. Absorption and scattering in ground-penetrating radar: Analysis of the bishop tuff. *Journal of Geophysical Research*, 111(E6). <https://doi.org/10.1029/2005JE002619>.
- Hadjimitsis D.G., Agapiou A. & Themistocleous K., 2014. *Integrated Use of Space, Geophysical and Hyperspectral Technologies Intended for Monitoring Water Leakages in Water Supply Networks*. IntechOpen, London, UK.
- Halimshah N.N., Yusup A., Amin Z.M. & Ghazalli M.D., 2015. Visual inspection of water leakage from ground penetrating radar radargram. *SPRS Annals of the Photogrammetry, Remote Sensing and Spatial Information Sciences*, II-2/W2, 191–198. <https://doi.org/10.5194/isprsannals-II-2-W2-191-2015>.
- Hawari A.A., Khader M., Zayed T. & Moselhi O., 2016. Detection of leaks in water mains using ground penetrating radar. *International Journal of Geological and Environmental Engineering*, 10(4), 422–425.
- Hunaidi O. & Giamou P., 1998. Ground-penetrating radar for detection of leaks in buried plastic water distribution pipes. [in:] *Seventh International Conference on Ground Penetrating Radar: May 27–30, 1998, University of Kansas, Lawrence, Kansas, USA: Proceedings*, Radar Systems and Remote Sensing Laboratory, University of Kansas, 783–786.
- Lai W.W.L., Chang R.K.W., Sham J.F.C. & Pang K., 2016. Perturbation mapping of water leak in buried water pipes via laboratory validation experiments with high-frequency ground penetrating radar (GPR). *Tunnelling and Underground Space Technology*, 52, 157–167. <https://doi.org/10.1016/j.tust.2015.10.017>.
- Muller K., 2005. *Modelling of GPR Wave Propagation and Scattering in Inhomogeneous Media*. Department of Geosciences, University of Oslo [M.Sc. thesis].
- Nakhkash M. & Mahmood-Zadeh M.R., 2004. Water leak detection using ground penetrating radar. [in:] *Proceedings of the Tenth International Conference on Ground Penetrating Radar: GPR 2004, Delft, The Netherlands, 21–24 June 2004*, Delft University of Technology, Delft, 525–528. <https://doi.org/10.1109/ICGPR.2004.179793>.
- Pilcher R., Hamilton S., Chapman H., Ristovski B. & Stapely S., 2007. *Leak Location and Repair: Guidance Notes*. International Water Association (IWA), London.
- Plewa M. & Plewa S., 1992. *Petrofizyka*. Wydawnictwa Geologiczne, Warszawa.
- PN-EN ISO 14688-1:2006. *Badania geotechniczne – Oznaczanie i klasyfikowanie gruntów – Część 1: Oznaczanie i opis*. Polski Komitet Normalizacyjny, Warszawa.
- Ponti C., Santarsiero M. & Schettini G., 2020. Time-domain electromagnetic scattering by buried dielectric objects with the cylindrical-wave approach for GPR modelling. *Electronics*, 9(3), 421. <https://doi.org/10.3390/electronics9030421>.
- Porubiaková A. & Komačka J., 2015. A comparison of dielectric constants of various asphalts calculated from time intervals and amplitudes. *Procedia Engineering*, 111, 660–665. <https://doi.org/10.1016/j.proeng.2015.07.129>.
- Puust R., Kapelan Z., Savic D.A. & Koppel T., 2010. A review of methods for leakage management in pipe networks. *Urban Water Journal*, 7(1), 25–45. <https://doi.org/10.1080/15730621003610878>.
- Radzevicius S.J. & Daniels J.J., 2000. Ground penetrating radar polarization and scattering from cylinders. *Journal of Applied Geophysics*, 45(2), 111–125. [https://doi.org/10.1016/S0926-9851\(00\)00023-9](https://doi.org/10.1016/S0926-9851(00)00023-9).
- Saarenketo T., 2003. *Measuring Electromagnetic Properties of Asphalt for Pavement Quality Control and Defect Mapping*. Roadscanners, Rovaniemi, Finland.
- Stampolidis A., Soupios P., Vallianatos F. & Tsokas G.N., 2003. Detection of leaks in buried plastic water distribution pipes in urban places – A case study. [in:] *Proceedings of the 2nd International Workshop on Advanced Ground Penetrating Radar: May 14–16, 2003, AULA, Delft, the Netherlands*, International Research Centre for Telecommunications-transmission and Radar, Delft, 120–124. <https://doi.org/10.1109/AGPR.2003.1207303>.
- Ustawa z dnia 7 lipca 1994 r. – Prawo budowlane* [The Act of 7 July 1994 – Construction Law]. Dz.U. 1994 nr 89 poz. 414.
- Wutke M., Lejzerowicz A., Jackiewicz-Rek W., Garbacz A., 2019. Influence of variability of water content in different states on electromagnetic waves parameters affecting accuracy of GPR measurements of asphalt and concrete pavements. *MATEC Web of Conferences*, 262, 06012. <https://doi.org/10.1051/mateconf/201926206012>.
- Yang Y., Du Z., Li Y., Zhang T., Liu L., Iqbal I. & Peng S., 2022. Anomaly detection of pipeline leakage based on electric field component imaging using ground penetrating radar. *Advances in Civil Engineering*, 1799750. <https://doi.org/10.1155/2022/1799750>.
- Yee K.S., 1966. Numerical solution of initial boundary value problems involving Maxwell's equations in isotropic media. *IEEE Transactions on Antennas and Propagation*, 14(3), 302–307. <https://doi.org/10.1109/TAP.1966.1138693>.
- Ying L., Li-Xin G. & Li-Ying F., 2019. GPR echo analysis of compound scattering of underground rough surface and multiple objects. [in:] *2019 IEEE International Conference on Computational Electromagnetics: ICCEM 2019: Proceedings: March 20–22, 2019, Shanghai, China*, IEEE, Piscataway, 1–3. <https://doi.org/10.1109/COMPEM.2019.8778908>.